Thin Solid Films 699 (2020) 137906

Contents lists available at ScienceDirect

Thin Solid Films

journal homepage: www.elsevier.com/locate/tsf

Determining effective crack lengths from electrical measurements in polymer-supported thin films

O. Glushko[a,b,*], B. Putz[a,1], M.J. Cordill[a,b]

[a] Erich Schmid Institute of Materials Science, Austrian Academy of Sciences, Jahnstrasse 12, 8700 Leoben, Austria
[b] Department of Materials Physics, Montanuniversität Leoben, Jahnstrasse 12, 8700 Leoben, Austria

ARTICLE INFO

Keywords:
Thin films
Polymer substrate
Crack length
Crack density
Electrical resistance
Tensile test

ABSTRACT

Although it is evident that the formation of multiple through-thickness cracks in polymer-supported thin films leads to an increase of the electrical resistance, the attempts to quantify the dependence of resistance growth only based on the induced crack density have not yet been successful. In this paper a recently developed relationship, representing the resistance growth as a two-variable polynomial function of crack density and crack length, is utilized to analyze the crack patterns induced by monotonic and cyclic tensile loading of 250 nm thick Cu films with a 10 nm Cr adhesion layer on polyimide. It is demonstrated that by knowing the in-situ resistance during deformation and post-mortem linear density of induced cracks, it is possible to extract the effective crack lengths, a parameter which is often ignored during experimental characterization of the damage induced through mechanical loading. The described algorithm is not only much more cost-effective in comparison to time-consuming in-situ microscopy methods, it also reflects the reliability of the whole sample rather than of only selected surface areas.

1. Introduction

Polymer-supported metal thin films subjected to a mechanical load typically do not completely fracture, rather they exhibit multiple crack formation [1,2,11–15,3–10]. Therefore, additional in-situ techniques are required to track structural changes within the film during mechanical testing. Structural changes in the film can be observed by performing mechanical in-situ tests under an optical light microscope, atomic force microscope or inside a scanning electron microscope (SEM). Alternatively, one can record the electrical resistance of the film during mechanical straining and correlate the resistance signal with the damage induced by mechanical strain. The in-situ resistance measurements have several striking advantages in comparison to in-situ microscopy techniques. First of all, in-situ resistance measurements can be easily performed with any tensile testing device while for in-situ microscopy experiments special compact tensile stages, typically having restricted functionality, are required. In-situ resistance measurements are fully automated which is especially important for fatigue experiments and experiments with high strain rates that may last several weeks or only a few seconds. Furthermore, the electrical resistance can provide information about the structural integrity of the entire sample in contrast to microscopy techniques, examining only a selected sample area. Finally, microscopy techniques typically capture the changes on the film surface while electric current flows through the film cross-section. For example, it was shown that strain-induced grain coarsening in Cu and Au films on polyimide can be detected by a decrease in the measured resistance with the number of applied tensile cycles [16–18].

Although the in-situ resistance measurements have been extensively used over the last decade, the correlation between the change of measured resistance and induced mechanical damage remained predominantly on a qualitative level, which can be expressed as “more extensive cracking leads to more significant resistance growth”. It is typically assumed that, under monotonic loading conditions, the critical strain corresponding to the propagation of through-thickness cracks (also frequently called the crack onset strain) corresponds to a deviation of the resistance growth from the constant volume approximation [1–5,13–15]. The constant volume approximation implies that the film deforms purely plastically without crack formation, material volume is conserved, and the resistance changes only due to the change of sample geometry, as shown in

$$\frac{R}{R_0} = \left(\frac{L}{L_0}\right)^2, \tag{1a}$$

where R is the resistance measured during straining, R_0 is the initial

* corresponding author.
E-mail addresses: oleksandr.glushko@unileoben.ac.at (O. Glushko), barbara.putz@empa.ch (B. Putz), megan.cordill@oeaw.ac.at (M.J. Cordill).
[1] now at Empa, Swiss Federal Laboratories for Materials Science and Technology, Feuerwerkerstrasse 39, 3602, Thun, Switzerland

https://doi.org/10.1016/j.tsf.2020.137906
Received 20 August 2019; Received in revised form 14 February 2020; Accepted 28 February 2020
Available online 29 February 2020
0040-6090/

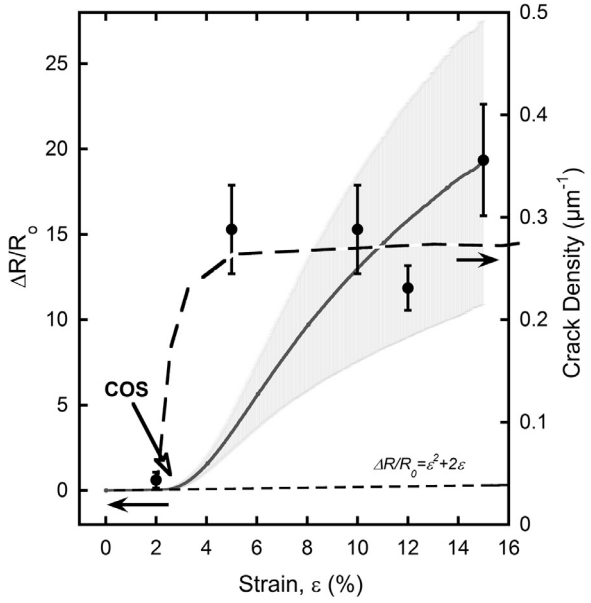

Fig. 1. Correlation of crack density (solid circles) and relative resistance ratio (solid line) as a function of applied strain for a 50 nm Au film with a 10 nm Cr interlayer on polyimide. The dashed line depicts approximate evolution of the crack density and has no mathematical meaning. Error bars represent the standard deviations of the measured crack density. Grey area shows the deviation of the measured resistance for five different samples. .

resistance, L is the apparent sample length during straining and L_0 is the initial sample length. Eqn. (1a) can be re-written in the following form, which will be required for further analysis:

$$\frac{\Delta R}{R_0} = \varepsilon^2 + 2\varepsilon, \tag{1b}$$

where $\Delta R = R\text{-}R_0$ and ε is the applied engineering strain.

The growth of the electrical resistance after reaching the crack onset strain is typically related to the formation of cracks, however, a clear correlation between the resistance signal and mechanical damage is still missing. As an illustrative example, Fig. 1 shows the crack density and the $\Delta R/R_0$ as a function of engineering strain for 50 nm Au films with a 10 nm Cr adhesion layer on polyimide (for more details see [19]). The crack onset strain (marked by "COS" in Fig. 1) correlates well with the rapid growth of the crack density, however, the resistance continues to increase monotonically even though the crack density saturates. The crack density between the applied strain of 5% and 15% changed insignificantly (from 0.29 ± 0.04 to 0.36 ± 0.05 μm^{-1}) but the resistance grew by 500%. This discrepancy of increasing electrical resistance and the saturation of the crack density is frequently observed for polymer-supported films [2,10,15,20–24].

Several models have been suggested to explain the resistance behavior as a function of cracking [6,8,21,25]. However, these models are lacking generality and were developed to explain behaviors of particular sample types in limited deformation ranges. For instance, to quantify the cracking of brittle indium tin oxide coatings on polymer substrates a model assuming the existence of conductive bridges inside the cracks was suggested [6–8]. Unfortunately, the nature of such potential bridges remained unexplored. Theoretical investigations on solids with a population of microcracks predicted an exponential dependence of electrical conductivity on the number of cracks per area and crack length [25]. Unfortunately, no experimental evidence of such a relationship was provided. Mora et al. [21] also proposed an exponential function with five fitting parameters to express the dependence of electrical resistance on crack density. Although it was possible to fit some parts of experimental curves by such a function, the general applicability of this model is questionable. In the recent model [26] the resistance growth was represented as a two-variable polynomial function of crack length and crack density. Although a simple comparison of model and experiment was provided in [26], it was not proved that the model could be generally applied to different material systems.

Apart from the apparent lack of models explaining correlations between the parameters of crack patterns and resistance growth, in many cases through-thickness cracks can be hardly identified using microscopy techniques. For example, the cracks induced by cyclic straining (fatigue damage) of ductile films are typically running inside the extrusions and cannot be clearly resolved by examination of the top surface of the film. More generally, deduction of through-thickness crack densities from microscopic images of the film surface can be ambiguous. It is not always clear which surface feature should be interpreted as a through-thickness crack and which should be attributed to a local deformation of different type (e.g. slip band, extrusion, neck) without additional time consuming cross-sections made with focused ion beam techniques. If the crack density is calculated manually from the surface images then this decision is dependent on the person performing the analysis. If a computer algorithm is used then any local change in brightness or contrast of the image may influence the evaluation. Also, images of the same sample surface taken at different magnifications could be interpreted differently. Electrical resistance, in contrast, is an objectively measured quantity which does not require time- or cost-expensive experiments and can be used as a universal measure of thin film cracking. Therefore, combining post-straining microscopy analysis with auxiliary information about the crack pattern extracted from electrical resistance is necessary to better understand the fracture of polymer-supported films.

The aim of this study is to demonstrate how the electrical resistance recorded in-situ during mechanical testing can be utilized for a quantitative description of the effective crack length. By means of a recently reported explicit relationship between the resistance growth and the density and lengths of induced cracks [26], different crack patterns observed in 250 nm thick copper films on polyimide substrates are analyzed. It is shown that by combining the final crack density from post-mortem scanning electron microscopy (SEM) micrographs with the in-situ resistance data, the effective lengths of through-thickness cracks at different stages of deformation can be determined. This provides a clear understanding of how resistance growth and through-thickness crack propagation occur in thin films on polymer substrates. Moreover, the resistance recovery during sample unloading can be clearly related to crack re-bridging due to viscoelastic relaxation of the polymer substrate.

2. Theoretical background

Until recently the quantitative relationship between resistance growth and crack pattern parameters was unexplored. In a recent publication [26] a quantitative relationship was deduced with the help of finite element modeling. The growth of electrical resistance was shown to be a function of two independent variables: the areal crack density and the crack length. Since it is difficult to unambiguously determine the areal crack density experimentally, the same relationship is more useful in the following form, using the linear crack density [26]:

$$\frac{R^*}{R_0^*} = 1 + \frac{1}{\sqrt{2}} C_l l_0 + \frac{1}{2} C_l^2 l_0^2 \tag{2}$$

where R^* is the resistance of the film with cracks, R_0^* is the resistance of the sample with the same dimensions but without cracks, C_l is the linear crack density, and l_0 is the length of a single crack. The model assumes that all cracks have the same length, are oriented parallel to each other and perpendicular to the direction of electric current flow. It is also assumed that the cracks are through-thickness such that no current can flow through a crack, and that the crack lengths are much smaller than the sample width [26].

To provide a clear and simple algorithm of the crack pattern

description on the basis of the electrical signal, let us first simplify Eqn. (2). The linear crack density, C_l and the crack length, l_o, can be combined into a single factor, which will be called the cracking factor, C_F,

$$C_F = C_l\, l_0 = \frac{l_0}{\lambda}, \tag{3}$$

where λ is the average distance between cracks (crack spacing). According to Eqn. (3), the cracking factor is a dimensionless quantity and is equal to the ratio of the effective crack length to the crack spacing. Using Eqn. (3) and rewriting Eqn. (2) by taking into account that $R^*/R_0^* = 1 + \Delta R^*/R_0^*$ one can obtain the following quadratic equation:

$$\frac{1}{2}C_F^2 + \frac{1}{\sqrt{2}}C_F - \frac{\Delta R^*}{R_0{}^*} = 0 \tag{4}$$

The positive solution of Eqn. (4) provides an expression for the cracking factor as a function of the electrical resistance growth:

$$C_F = \frac{1}{\sqrt{2}}\left(\sqrt{1 + 4\frac{\Delta R^*}{R_0{}^*}} - 1\right) \tag{5}$$

Eqn. (5) allows for the estimation of the cracking factor on the basis of the electrical resistance and vice versa. Visualization of Eqn. (5) reveals a few critical points which can help to deduce some simple "rules of thumb" (Fig. 2). A cracking factor of 1 indicates a crack pattern where the effective crack length equals the crack spacing and corresponds to the growth of the electric resistance by 120%. For the resistance growth of 20%, which is often considered as a tolerance value for electrical degradation [5], the corresponding cracking factor is about 0.25. This cracking factor value indicates that, on average, the cracks are separated by a distance four times larger than the crack length.

3. Experimental

Copper films with a thickness of 250 nm were deposited on 50 μm polyimide (UPILEX®) substrates by electron beam evaporation in a Balzers BAK 550 evaporation machine with a base pressure of 2.1×10^{-7} hPa and using a deposition rate of 0.3 nm/s. In order to have good adhesion to the PI substrate, a 10 nm Cr interlayer was used. The test samples with the width of 4 mm and length of 40 mm were cut out of larger sheets using a scalpel. Mechanical testing was performed on an MTS Tytron 250 uniaxial tensile testing device using a gauge length of 20 mm. Monotonic loading was applied at a strain rate of $2.5 \times 10^{-4}\ s^{-1}$ to maximum engineering strains of 20% and 40% using separate samples for each experiment. Cyclic tensile loading was applied in strain control mode by means of a sine strain function oscillating between the initial position (zero strain) and a defined value of maximum engineering strain. The frequency of the sine strain function was 0.5 Hz and the maximum engineering strain values reviewed in this paper are 1% and 2%. Mechanical strain was measured using the extensometer of the tensile testing device and all strain values stated herein refer to the engineering strain. Electrical resistance was recorded in-situ with a four point probe geometry using electrical contacts incorporated directly into the straining grips during loading and unloading [27]. Post-mortem SEM characterization was performed on a Zeiss Leo 1525 (5 kV, 30 μm aperture) one to seven days after testing to ensure fully relaxed samples [14]. The linear crack densities, C_l, were measured using at least 10 SEM images containing altogether more than 100 cracks. Resistance signal and crack density are taken from the same sample to have a 1 to 1 correlation between the resistance and crack density data.

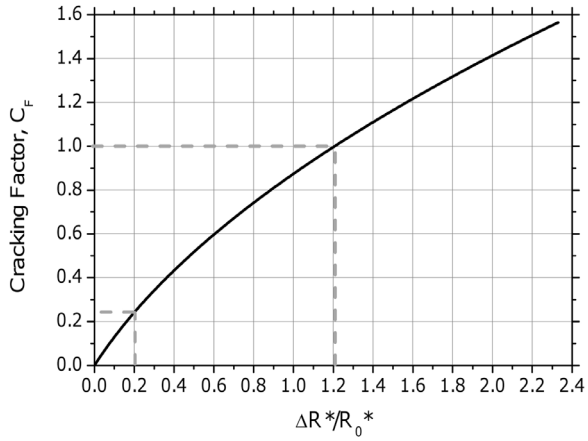

Fig. 2. The dependence of the cracking factor, C_F, on the increase in electrical resistance calculated according to Eqn. (5). The gray dashed curves depict the two special cases described in the text.

It is important to note that the normalized resistance growth $\Delta R^*/R_0{}^*$ in Eqns. (2)–(5) represents the ratio of resistance growth caused by the formation of cracks compared to the resistance of the sample with the same dimensions but without cracks [26]. In contrast, experimentally measured resistance is normalized to the resistance of an undeformed sample having initial dimensions. In order to make the two definitions of resistance growth consistent with each other, experimentally measured resistance at a given strain value should be reduced by the constant volume approximation value calculated for the same strain. This corresponds to the subtraction of the constant volume approximation curve (Eqn. (1b)) from the experimentally measured resistance curve. An example of such a modification of in-situ resistance is shown in Fig. 3, where each measured resistance value (black curve) at a given engineering strain, ε, is reduced by $\varepsilon^2 + 2\varepsilon$ (red curve).

4. Results and discussion

4.1. Monotonic tensile straining

In-situ resistance curves recorded during monotonic tensile loading of the Cu/Cr film system on polyimide to the engineering strains of 20% and 40% are shown in Fig. 4. The constant volume approximation was subtracted from the measured curves as previously described. As follows from Fig. 4, the films deform plastically without forming through-thickness cracks up to the engineering strain of approximately 10%. At engineering strains higher than 10% the resistance increases, indicating the formation and propagation of through-thickness cracks. During and after unloading, a resistance decrease is observed and final values of the

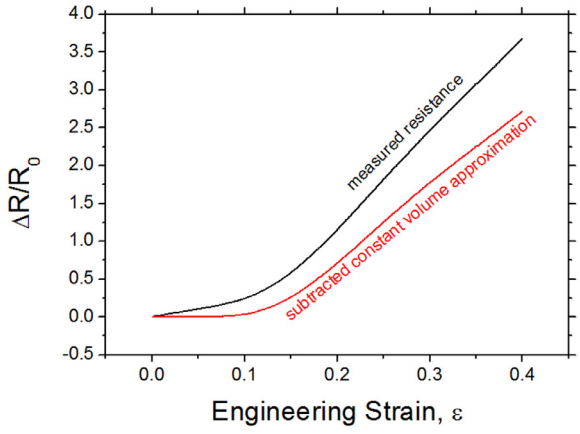

Fig. 3. Example of the difference between the measured resistance (black curve) and the modified resistance ($\Delta R^*/R_0{}^*$) after the subtraction of the constant volume approximation (red curve). (For interpretation of the references to color in this figure legend, the reader is referred to the web version of this article.)

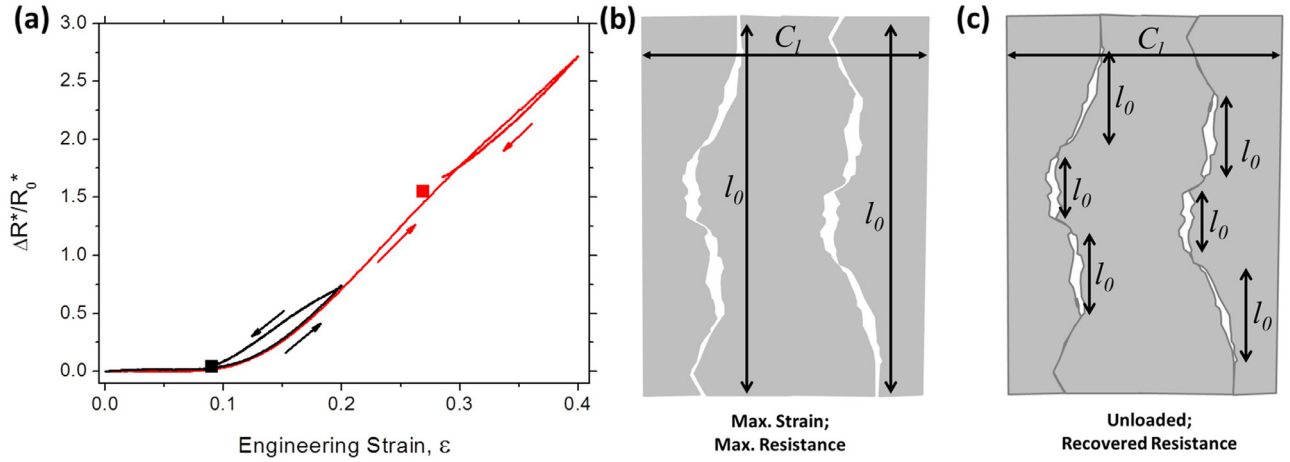

Fig. 4. (a) Resistance behavior of 250 nm thick Cu films with a 10 nm Cr adhesion layer on polyimide under monotonic tensile loading to 20% and 40% engineering strain. After 20% strain full resistance recovery (black square) and after 40% strain, partial resistance recovery (red square) were observed. A schematic diagram of a crack at maximum strain of 40% is shown in (b). The same crack in an unloaded state having lower resistance due to crack re-bridging is schematically depicted in (c). (For interpretation of the references to color in this figure legend, the reader is referred to the web version of this article.)

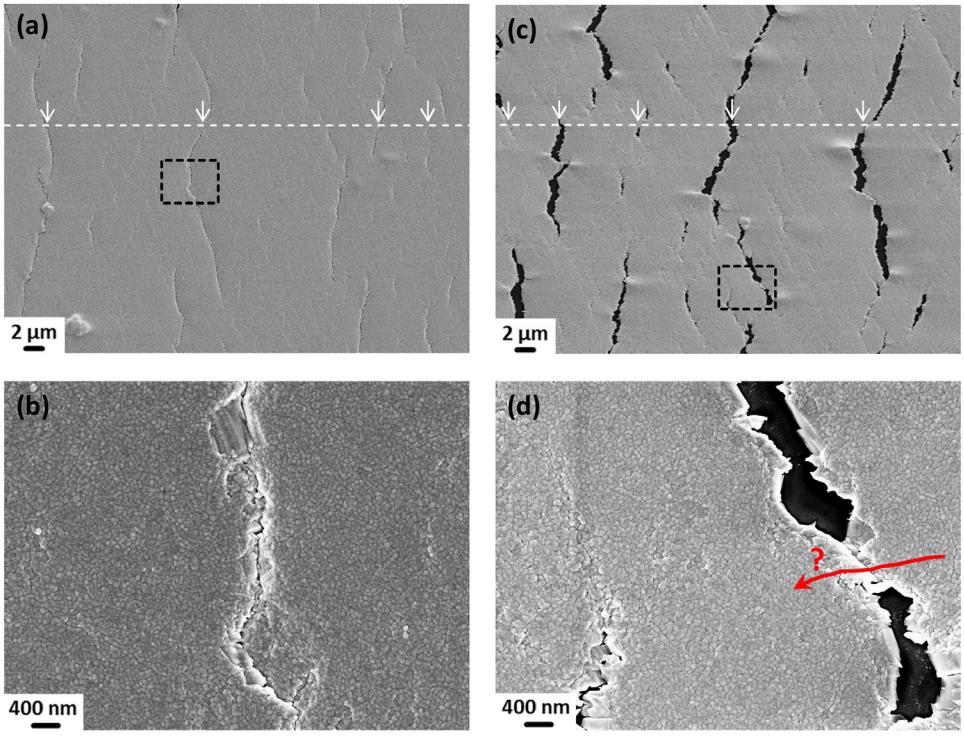

Fig. 5. Post-mortem SEM micrographs of the surface of 250 nm thick Cu films with a 10 nm Cr adhesion layer on polyimide after straining to 20% (a,b) and 40% (c,d). The micrographs (b) and (d) are enlarged images of the areas marked by dashed rectangles in (a) and (c), respectively. The horizontal white dashed lines with arrows in (a) and (c) demonstrate how the linear deformation density from one image is deduced. The red arrow with a question mark in (d) depicts a potential bridge for the current flow. Straining was performed along the horizontal direction. (For interpretation of the references to color in this figure legend, the reader is referred to the web version of this article.)

unloaded samples recorded 30 min after straining are depicted by solid square symbols. It is important to note that virtually full resistance recovery is observed in the films strained to 20%. Post-mortem SEM images for both samples are shown in Fig. 5. After straining to 20% the film displays numerous areas of localized deformation (Fig. 5a). Due to the viscoelastic substrate relaxation it is difficult to unambiguously determine which localized deformations correspond to through-thickness cracks and which might be local plasticity events, such as necking or slip bands (Fig. 5b). After applying 40% engineering strain the film exhibits numerous open through-thickness cracks (Fig. 5c). Also in this case, the relaxation of the substrate during unloading leads to uncertainties in through-thickness crack characterization. For instance, the enlarged image in Fig. 5d shows a re-bridged crack which may or may not be conductive. A potential pathway for electrical current is shown by the arrow with a question mark (Fig. 5d). It can be concluded that the experimental measurement of crack lengths from the post-mortem SEM images cannot be performed with an acceptable accuracy. In contrast, the linear densities of the localized areas of deformation, also referred to as the deformation density as defined in [24,28], can be extracted relatively unambiguously as shown in Figs. 5a and 5c. The linear deformation density is defined as the number of intersections between the dashed line drawn parallel to the straining direction and localized deformations running perpendicular to the straining direction divided by the length of the dashed line. One can assume that the through-thickness crack density at a maximum applied strain and the deformation density in the unloaded state are similar and the resistance recovery is caused by the reduction of crack lengths. Such an assumption can be justified by the fact that at high strain the crack density typically saturates, as demonstrated in Fig. 1, thus the resistance growth is caused solely by an increase in the effective crack length [26].

Table. I
Summary of the cracking factors and effective cracks lengths determined with Eqns. (3) and 5.

	$\Delta R^*/R_0^*$@max strain	C_F (Eqn. (5)) @max strain	$\Delta R^*/R_0^*$unloaded	C_F (Eqn. (5)) unloaded	C_l, μm^{-1}	l_o (Eqn. (3)) @max strain	l_o (Eqn. (3)) unloaded
20% strain	0.74	0.7	0	0	0.068 ± 0.013	9–13 μm	0 μm
40% strain	2.72	1.73	1.55	1.2	0.079 ± 0.014	19–27 μm	13–18 μm

Therefore, during unloading we assumed that this process is reversed since the slope of the unloading curve is virtually the same as of the corresponding portion of the loading curve (Fig. 4a). This concept is visualized in Figs. 4b and 4c, where at the maximum strain and resistance, the long through-thickness cracks leading to the resistance increase are open (Fig. 4b). When the load is removed (Fig. 4c) portions of the through-thickness cracks can re-bridge and cause the reduction of the measured resistance due to the reduction of effective crack lengths.

From Figs. 4 and 5 one can measure all of the input parameters needed to determine the cracking factors and the effective crack lengths at the maximum applied strain and after unloading. Table I summarizes the results of the analysis performed for the two curves shown in Fig. 4. Experimental resistance growth at maximum strain ($\Delta R^*/R_0^*$@*maxstrain*) is used to calculate the corresponding cracking factor at the maximum engineering strain (C_F @ max strain) using Eqn. (5). The cracking factor in the unloaded state (C_F unloaded) is calculated from the corresponding unloaded electrical resistance values. Assuming that the crack density (C_l) experimentally determined from Fig. 5 (unloaded state) remains the same at the maximum applied strain and in the unloaded state, one can calculate the effective crack lengths (l_o) at both the maximum strain and after unloading. Since the values of crack lengths are usually widely distributed, a range of values for l_o is presented in Table I. The lower value is calculated using the experimental mean value of C_l plus the standard deviation and for the higher value of l_o the standard deviation was subtracted from the mean value of C_l. The analysis presented in Table I uncovers the correlations between the resistance growth and through-thickness crack propagation. At the maximum engineering strain of 20% the average effective crack lengths were in the range 9–13 μm, while after unloading all cracks have re-bridged resulting in an effective length close to zero. Effective lengths of the cracks at 40% engineering strain are 19–27 μm while after unloading the effective crack lengths decrease to 13–18 μm.

It is well-known from literature that the crack density of polymer-supported films subjected to tensile load usually saturates after some applied strain. This saturation is explained by the shear lag model [29,30] stating that on the edge of an existing crack the film stress is close to zero. The stress is then transferred from the substrate to the film and increases with the distance from the crack edge. At some distance from the crack edge, which depends on film thickness, the stress reaches a high enough value to induce the formation of another crack. Taking into account the shear lag model one can conclude that the crack density in the copper films is close to saturation after 20% engineering strain since there is only a small difference in crack density between the film strained to 20% and the film strained to 40% (Table I). Significant resistance increase between 20% and 40% strain (Fig. 4a) despite the approximately constant crack density (Table 1) can be clearly attributed to the increase of the effective crack length with increased strain.

4.2. Cyclic tensile straining

The in-situ resistance signal recorded during cyclic tensile straining of the Cu/Cr film system is depicted in Fig. 6. For the strain amplitude of 2% the resistance demonstrates a quick increase with the cycle number indicating the formation and propagation of through-thickness cracks. In the case of the 1% strain amplitude, the initial stage (first 2000–3000 cycles) is characterized by no significant change of resistance followed by gradual resistance growth with the cycle number. The post-mortem SEM images for the three cases considered in Fig. 6 are shown in Fig. 7. Typical fatigue-induced damage in the form of propagating extrusion/crack couples is observed in all cases. As one can see in Fig. 7, it is again possible to extract the linear densities of extrusion/crack couples from the SEM images, however, it is virtually impossible to detect where the cracks are open providing an obstacle for electrical current flow and where the cracks are bridged.

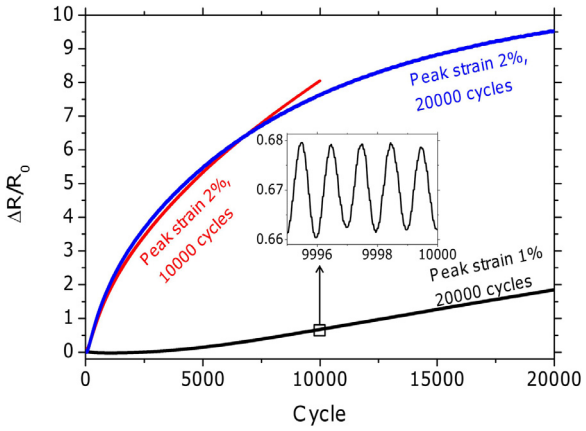

Fig. 6. The evolution of electrical resistance of the 250 nm thick Cu films with a 10 nm Cr adhesion layer on polyimide with number of applied tension cycles. Three curves correspond to cyclic strain of 1% up to 20,000 cycles (black), cyclic strain of 2% up to 10,000 cycles (red) and cyclic strain of 2% up to 20,000 cycles, according to the notation in the graph. The inset shows the fine structure of the resistance signal where each loading-unloading cycle can be clearly resolved. (For interpretation of the references to color in this figure legend, the reader is referred to the web version of this article.)

By analogy with the analysis presented for monotonic uniaxial tensile straining, the experimentally measured final values of $\Delta R/R_0$ are utilized to calculate the cracking factor by means of Eqn. (5) and the experimentally measured deformation densities are used to deduce the effective crack lengths (Table II). With the strain amplitudes of 1% and 2% the substrate stays in the elastic regime, thus, the sample dimensions do not change and $\Delta R/R_0$ is assumed to be equal to $\Delta R^*/R_0^*$. As follows from Table II, the differences in the resistance growth between the three samples are attributed to the differences in the measured deformation densities while the effective crack lengths are similar in all three considered cases. The differences in crack densities between 1% and 2% cyclic strain amplitudes can be explained by the different density of crack initiation sites actuated by different strain amplitudes. The fact that the crack lengths after 1% and 2% strain amplitude are similar is somewhat surprising, but can be explained by the crack shielding effect. In the case of 2% strain amplitude the density of propagating cracks is high and the cracks propagating in opposite directions more often mutually shield each other due to the reduced local stress, as described by the shear lag model. In the case of 1% strain amplitude, there are fewer cracks but they have more space to propagate before meeting another crack propagating in the opposite direction.

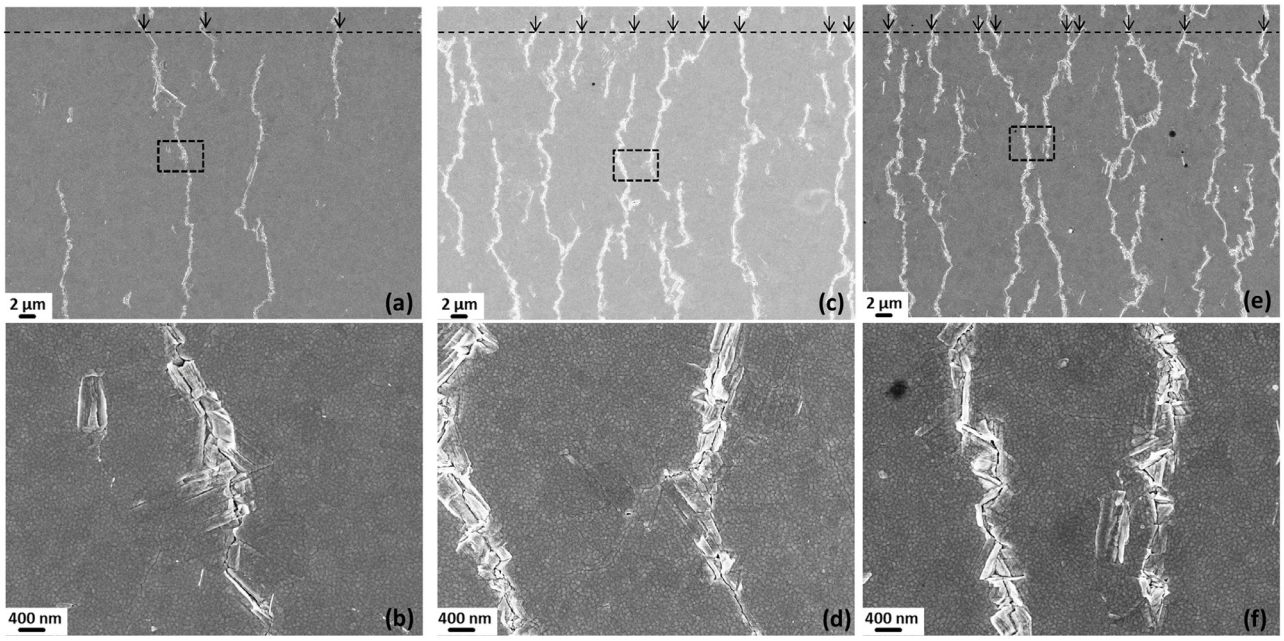

Fig. 7. Post-mortem SEM micrographs of the surface of 250 nm thick Cu films with a 10 nm Cr adhesion layer on polyimide after 20,000 cycles with 1% peak strain (a,b), 10,000 cycles with 2% peak strain (c,d), and 20,000 cycles with 2% peak strain (e, f). The micrographs (b), (d), and (f) are enlarged images of the areas marked by dashed rectangles in (a), (c), and (e), respectively. The horizontal black dashed lines with arrows in (a), (c), and (e) demonstrate how the crack/extrusion density from one image is deduced. Straining was performed along the horizontal direction.

Table. II
Summary of the cracking factors and effective cracks lengths determined with Eqns. (3) and 5 for cyclic tensile straining.

	$\Delta R/R_0$	C_F	C_l, μm^{-1}	lo
1%, 20,000 cycles	1.85	1.35	0.064 ± 0.015	17–27μm
2%, 10,000 cycles	8.1	3.34	0.135 ± 0.014	22–28μm
2%, 20,000 cycles	9.6	3.73	0.145 ± 0.012	24–28 μm

5. Summary and conclusions

With the rapid development of new materials and fabrication techniques for production of thin films on polymer substrates a fast, thorough, and reproducible method for electro-mechanical reliability characterization is required. In this study, an algorithm for quantitative characterization of thin film cracking based on the combined analysis of in-situ resistance and post-mortem microscopy is presented. It is shown how the effective lengths of the induced cracks can be estimated using the electrical resistance signal. Continuous monotonic growth of resistance despite the saturation of the crack density during monotonic uniaxial tensile testing is shown to be a direct consequence of an increase of the effective crack lengths. In contrast, for cyclic tensile loading with strain values below the crack onset strain, the differences in resistance growth are caused by different crack densities while similar effective crack lengths are observed. The 250 nm thick Cu film with a 10 nm Cr adhesion layer on polyimide used in this work acts as a model material system, but the presented method is expected to be universally applicable to different thin film systems as long as the cracks are through-thickness. The ability to calculate the cracking factor, which is the ratio of effective crack length to the average crack spacing, directly from the value of the recorded electrical resistance provides a unique possibility to characterize crack patterns in the cases where conventional microscopy cannot be applied, such as for buried films, films with high porosity or with high surface roughness.

Although for many applications cracking of a thin film means immediate functional failure, quantification of the relationship between the growth of electrical resistance and through-thickness crack propagation can provide important information about the material electro-mechanical properties. The effect of grain size, chemical composition, fabrication technique, film thickness or interface properties could be further evaluated with better knowledge of how the electrical resistance corresponds to the crack or deformation densities and crack lengths with increasing strain or cycle number.

CRediT authorship contribution statement

O. Glushko: Conceptualization, Methodology, Visualization, Investigation, Writing - original draft, Writing - review & editing. **B. Putz:** Validation, Visualization, Writing - review & editing. **M.J. Cordill:** Visualization, Writing - review & editing.

Declaration of Competing Interests

The authors declare that they have no known competing financial interests or personal relationships that could have appeared to influence the work reported in this paper. https://doi.org/10.13039/501100002428

Acknowledgments

The authors acknowledge support by the Austrian Science Fund (FWF), project P27432-N20. Additional support was provided through the European Research Council under the ERC Advanced Grant INTELHYB grant ERC-2013-ADG-340025).

References

[1] F. Macionczyk, W. Brückner, Tensile testing of ALCu thin films on polyimide foils, J. Appl. Phys. 86 (1999) 4922–4929, https://doi.org/10.1063/1.371461.
[2] R.M. Niu, G. Liu, C. Wang, G. Zhang, X.D. Ding, J. Sun, Thickness dependent critical strain in submicron Cu films adherent to polymer substrate, Appl. Phys. Lett. (2007) 90, https://doi.org/10.1063/1.2722684.
[3] N. Lu, X. Wang, Z. Suo, J.J. Vlassak, Metal films on polymer substrates stretched beyond 50%, Appl. Phys. Lett. 91 (2007), https://doi.org/10.1063/1.2817234 221909–221903.
[4] N. Lu, Z. Suo, J.J. Vlassak, The effect of film thickness on the failure strain of

polymer-supported metal films, Acta Mater. 58 (2010) 1679–1687, https://doi.org/10.1016/j.actamat.2009.11.010.
[5] G.D. Sim, S. Won, C.Y. Jin, I. Park, S.B. Lee, J.J. Vlassak, Improving the stretchability of as-deposited Ag coatings on poly-ethylene-terephthalate substrates through use of an acrylic primer, J. Appl. Phys. 109 (2011) 1–6, https://doi.org/10.1063/1.3567917.
[6] D. Cairns, R.W. II, D. Sparacin, S. Sachsman, Strain-dependent electrical resistance of tin-doped indium oxide on polymer substrates, Appl. Phys. Lett. 76 (2000) 2000–2002. http://scholar.google.com/scholar?hl=en&btnG=Search&q=intitle:Strain-dependent+electrical+resistance+of+tin-doped+indium+oxide+on+polymer+substrates#0 accessed May 29, 2012.
[7] Y. Leterrier, L. Médico, F. Demarco, J.A.E. Månson, U. Betz, M.F. Escolà, M.K. Olsson, F. Atamny, Mechanical integrity of transparent conductive oxide films for flexible polymer-based displays, Thin Solid Films 460 (2004) 156–166, https://doi.org/10.1016/j.tsf.2004.01.052.
[8] Y. Leterrier, A. Pinyol, L. Rougier, J.H. Waller, J.-A.E. Månson, Electro-fragmentation modeling of conductive coatings on polymer substrates, J. Appl. Phys. 106 (2009) 113508, , https://doi.org/10.1063/1.3266001.
[9] S. Merilampi, T. Laine-Ma, P. Ruuskanen, The characterization of electrically conductive silver ink patterns on flexible substrates, Microelectron. Reliab. 49 (2009) 782–790, https://doi.org/10.1016/j.microrel.2009.04.004.
[10] F.F. Schlich, A. Wyss, H. Galinski, R. Spolenak, Cohesive and adhesive properties of ultrathin amorphous and crystalline $Ge_2Sb2Te5$ films on polyimide substrates, Acta Mater. (2016), https://doi.org/10.1016/j.actamat.2016.12.060.
[11] A. Pinyol, B. Meylan, D. Gilliéron, V. Mewani, Y. Leterrier, J.-A.E. Månson, Electro-fragmentation analysis of dielectric thin films on flexible polymer substrates, Thin Solid Films 517 (2009) 2000–2006, https://doi.org/10.1016/j.tsf.2008.10.074.
[12] B. Erdem Alaca, M.T.A. Saif, H. Sehitoglu, On the interface debond at the edge of a thin film on a thick substrate, Acta Mater. 50 (2002) 1197–1209, https://doi.org/10.1016/S1359-6454(01)00421-9.
[13] M.M. Hamasha, K. Alzoubi, J.C. Switzer, S. Lu, S.B. Desu, M. Poliks, A study on crack propagation and electrical resistance change of sputtered aluminum thin film on poly ethylene terephthalate substrate under stretching, Thin Solid Films 519 (2011) 7918–7924, https://doi.org/10.1016/j.tsf.2011.06.062.
[14] O. Glushko, V.M. Marx, C. Kirchlechner, I. Zizak, M.J. Cordill, Recovery of electrical resistance in copper films on polyethylene terephthalate subjected to a tensile strain, Thin Solid Films 552 (2014) 141–145, https://doi.org/10.1016/j.tsf.2013.12.055.
[15] F.F. Schlich, R. Spolenak, Size- and phase-dependent mechanical properties of ultrathin Si films on polyimide substrates, Acta Mater. 110 (2016) 122–130, https://doi.org/10.1016/j.actamat.2016.03.028.
[16] O. Glushko, M.J. Cordill, Electrical resistance decrease due to grain coarsening under cyclic deformation, Jom 66 (2014) 598–601, https://doi.org/10.1007/s11837-014-0943-x.
[17] O. Glushko, M.J. Cordill, A. Klug, E.J.W. List-Kratochvil, The effect of bending loading conditions on the reliability of inkjet printed and evaporated silver metallization on polymer substrates, Microelectron. Reliab. 56 (2016) 109–113, https://doi.org/10.1016/j.microrel.2015.10.007.
[18] M.J. Cordill, O. Glushko, A. Kleinbichler, B. Putz, D.M. Többens, C. Kirchlechner, Microstructural influence on the cyclic electro-mechanical behaviour of ductile films on polymer substrates, Thin Solid Films 644 (2017) 166–172, https://doi.org/10.1016/j.tsf.2017.06.067.
[19] B. Putz, R.L. Schoeppner, O. Glushko, D.F. Bahr, M.J. Cordill, Improved electro-mechanical performance of gold films on polyimide without adhesion layers, Scr. Mater. 102 (2015) 23–26, https://doi.org/10.1016/j.scriptamat.2015.02.005.
[20] L. Rebouta, L. Rubio-Peña, C. Oliveira, S. Lanceros-Mendez, C.J. Tavares, E. Alves, Strain dependence electrical resistance and cohesive strength of ITO thin films deposited on electroactive polymer, Thin Solid Films 518 (2010) 4525–4528, https://doi.org/10.1016/j.tsf.2009.12.022.
[21] A. Mora, K.A. Khan, T. El Sayed, Prediction of crack density and electrical resistance changes in indium tin oxide/polymer thin films under tensile loading, Int. J. Damage Mech. 24 (2015) 546–561, https://doi.org/10.1177/1056789514539362.
[22] T. Jörg, D. Music, F. Hauser, M.J. Cordill, R. Franz, J. Winkler, J.M. Schneider, C. Mitterer, Deformation behavior of *Re* alloyed Mo thin films on flexible substrates : in situ fragmentation analysis supported by first-principles calculations, Sci. Rep. 7 (2017), https://doi.org/10.1038/s41598-017-07825-1 7374-1–10.
[23] B. Putz, O. Glushko, V.M. Marx, C. Kirchlechner, D. Toebbens, M.J. Cordill, Electro-mechanical performance of thin gold films on polyimide, MRS Adv. (2016) 773–778, https://doi.org/10.1557/adv.2016.233.
[24] M.J. Cordill, O. Glushko, J. Kreith, V.M. Marx, C. Kirchlechner, Measuring electro-mechanical properties of thin films on polymer substrates, Microelectron. Eng. 137 (2015) 96–100, https://doi.org/10.1016/j.mee.2014.08.002.
[25] S. Giordano, Electrical behaviour of a single crack in a conductor and exponential laws for conductivity in micro cracked solids, Int. J. Appl. Electromagn. Mech. 26 (2007) 1–19.
[26] O. Glushko, P. Kraker, M.J. Cordill, Explicit relationship between electrical and topological degradation of polymer-supported metal films subjected to mechanical loading, Appl. Phys. Lett. 110 (2017) 1–5, https://doi.org/10.1063/1.4982802.
[27] O. Glushko, M.J. Cordill, Electrical resistance of metal films on polymer substrates under tension, Exp. Tech. 40 (2016) 303–310, https://doi.org/10.1007/s40799-016-0040-x.
[28] M.J. Cordill, V.M. Marx, Fragmentation testing for ductile thin films on polymer substrates, Philos. Mag. Lett 93 (2013) 618–624, https://doi.org/10.1080/09500839.2013.830792.
[29] C.H. Hsueh, M. Yanaka, Multiple film cracking in film/substrate systems with residual stresses and unidirectional loading, J. Mater. Sci. 38 (2003) 1809–1817, https://doi.org/10.1023/A:1023200415364.
[30] F. Ahmed, K. Bayerlein, S.M. Rosiwal, M. Göken, K. Durst, Stress evolution and cracking of crystalline diamond thin films on ductile titanium substrate: analysis by micro-Raman spectroscopy and analytical modelling, Acta Mater. 59 (2011) 5422–5433, https://doi.org/10.1016/j.actamat.2011.05.015.